RSC Advances

PAPER

View Article Online
View Journal | View Issue

Cite this: *RSC Adv.*, 2025, **15**, 357

The scavenging mechanism of hydrazone compounds towards HOO˙ and CH_3OO˙ radicals: a computational mechanistic and kinetic study†

Chhinderpal Kaur and Debasish Mandal *

In this study, a detailed DFT investigation was conducted to systematically analyze the scavenging activity of six hydrazone compounds (**1–6**) against HOO˙ and CH_3OO˙ radicals. Three mechanistic pathways were explored: hydrogen atom transfer (HAT), single electron transfer followed by proton transfer (SETPT), and sequential proton loss electron transfer (SPLET). These mechanisms were evaluated based on thermodynamic parameters, including bond dissociation enthalpy (BDE), ionization potential (IP), proton dissociation enthalpy (PDE), proton affinity (PA), and electron transfer enthalpy (ETE) in the gas phase, water, and pentyl ethanoate. HAT was identified as the most favorable mechanism in the gas phase, while SPLET was preferred in water. Among the studied compounds, compound **2** showed the highest rate constants for HOO˙ scavenging following the HAT mechanism in the gas phase observed at the O2′–H bond with a k_{Eck} value of 6.02×10^4 M^{-1} s^{-1}. For CH_3OO˙ scavenging, the same compound exhibited the highest rate constants at the N8–H (9.03×10^4 M^{-1} s^{-1}) and O2′–H (7.22×10^4 M^{-1} s^{-1}) sites. The calculated overall rate constant values of compound **2** are $k_{overall}$ (HOO˙) $= 6.86 \times 10^4$ M^{-1} s^{-1} and $k_{overall}$ (CH_3OO˙) $= 1.63 \times 10^5$ M^{-1} s^{-1}. These results suggest that compound **2** exhibits antioxidant activities comparable to butylated hydroxyanisole (BHA), consistent with experimental findings, indicating its potential as an effective scavenger of hydroperoxyl and methoxy peroxyl radicals. In aqueous solution, the anionic form of compound **2** showed the greatest HOO˙ and CH_3OO˙ radical scavenging activity among all of the studied compounds with rate constants of $k_{app} = 1.8 \times 10^7$ M^{-1} s^{-1} and $k_{app} = 3.3 \times 10^6$ M^{-1} s^{-1}, respectively. Compared with some typical antioxidants such as rubiadin, natural fraxin, and natural anthraquinones, compound **2** showed higher HOO˙ and CH_3OO˙ radical scavenging activity in water. Thus, compound **2** is a promising antioxidant in aqueous physiological environments.

Received 25th October 2024
Accepted 17th December 2024

DOI: 10.1039/d4ra07625g

rsc.li/rsc-advances

Introduction

Oxidative stress, which results from an imbalance between the production and consumption of reactive oxygen species (ROS) in biological systems, has become a critical health concern.[1] Excessive ROS generation contributes significantly to the development of chronic and degenerative diseases, including cancer, heart failure, cardiovascular disorders, autoimmune conditions, arthritis, and Alzheimer's disease.[2,3] ROS, such as hydroxyl radicals (HO˙), peroxyl radicals (ROO˙), superoxide anions ($O^{2\cdot-}$), and non-free-radical species like singlet oxygen ($^1O_2$), are continuously produced in the body through various cellular metabolic processes, including NADPH oxidase reactions, cellular respiration, and electron transfer *via* cytochrome P450 systems, as well as from exposure to UV radiation.[4–6] Among these, peroxyl radicals (ROO˙) are particularly toxic due to their selective attack on biological molecules like proteins, DNA, and lipids.[7,8] However, these harmful effects can be mitigated by antioxidants, which neutralize free radicals by converting them into stable products.[9] Antioxidants prevent the initiation and propagation of radical reactions, ultimately slowing the oxidation process.[10] Numerous studies have explored effective antioxidants and their mechanisms of action.[11,12] Both synthetic and natural antioxidants demonstrate the ability to prevent cellular damage by scavenging ROS.[13–15]

Hydrazones are an important class of organic compounds that have garnered significant attention in medicinal chemistry due to their wide range of pharmacological properties, which can be harnessed to prevent and treat diseases associated with oxidative stress.[16] Hydrazones containing the azomethine group (–NH–N=CH–) form a hydrazide-like moiety (–C(=O)–NH–N=CH–) when linked to a carbonyl group.[17] This structure exhibits high reactivity due to the nucleophilic nature of the nitrogen atoms and the combined electrophilic and nucleophilic character of the carbon atom.[18] These hydrazone derivatives have demonstrated various biological activities, including anticancer,[19] antioxidant,[20–24] antidepressant,[25] antitubercular,[26]

Department of Chemistry and Biochemistry, Thapar Institute of Engineering and Technology, Patiala-147004, Punjab, India. E-mail: debasish.mandal@thapar.edu

† Electronic supplementary information (ESI) available. See DOI: https://doi.org/10.1039/d4ra07625g

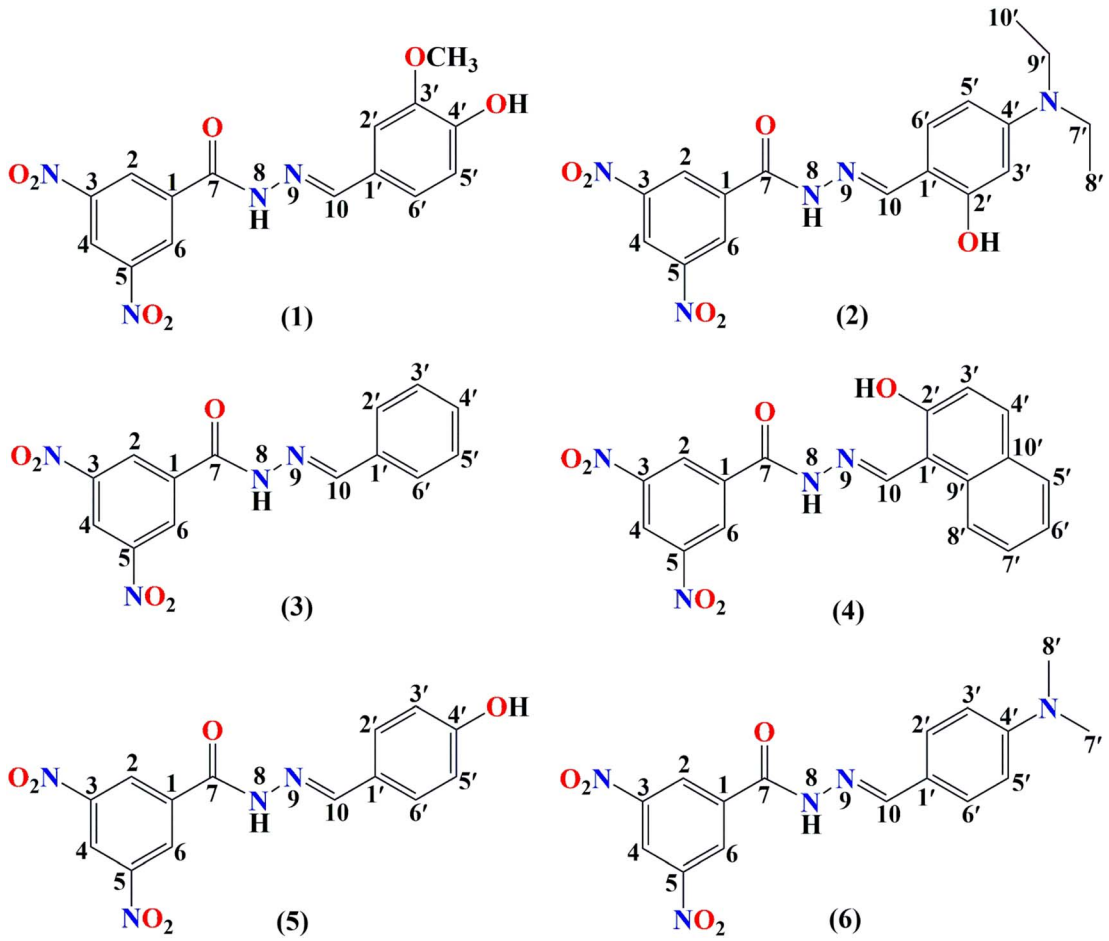

Fig. 1 2D molecular structures of hydrazone compounds *N*′–(4-hydroxy-3-methoxybenzylidene)-3,5-dinitrobenzohydrazide (**1**), *N*′–(4-(diethylamino)-2-hydroxy-benzylidene)-3,5-dinitrobenzohydrazide (**2**), *N*′-benzylidene-3,5-dinitrobenzohydrazide (**3**), *N*′–((2-hydroxynaphthalen-1-yl)methylene)-3,5-dinitrobenzohydrazide (**4**), *N*′–(4-hydroxybenzylidene)-3,5-dinitrobenzohydrazide (**5**), and *N*′–(4-(dimethylamino) benzylidene)-3,5-dinitrobenzohydrazide (**6**).

anti-inflammatory,[27] and anti-Alzheimer's effects.[28] Additionally, they have also demonstrated potent antioxidant properties, which are largely attributed to the presence of the crucial N–H bond.[17,29]

In this study, we have focused on the scavenging mechanism and kinetics of six promising heterocyclic hydrazone derivatives, which are presented in Fig. 1.

Başaran *et al.* synthesized the aforementioned hydrazone derivatives and assessed their antioxidant activity experimentally.[28] They demonstrated that these synthesized compounds have promising properties as antioxidant agents. The authors determined that compound **2** has better antioxidant activity than BHA among the studied compounds, whereas compounds **1** and **4** exhibited antioxidant activity close to that of BHA. Previous studies successfully used computational approaches to explore structure–activity relationships and guide the development of more potent antioxidants.[15,30,31] The experimental findings showed promising activity, prompting a yet-to-be-conducted theoretical investigation.

Herein, a systematic DFT study of the radical scavenging mechanism of hydrazone compounds (**1–6**), focusing on frontier molecular orbitals, molecular descriptors, and key thermodynamic parameters, has been presented. Solvent effects in polar (water) and nonpolar (pentyl ethanoate) media were also considered. Thermodynamic and kinetic analyses of the reactions with HOO˙ and CH_3OO˙ radicals were investigated using potential energy surfaces.

Computational details

All calculations were performed using the Gaussian 16 program suite.[32] Geometry optimizations were carried out with the DFT-M06-2X functional[33] and 6-311+G(d,p) basis set, which is a reliable method for studying radical thermodynamics and kinetics.[34–38] Harmonic vibrational frequencies were calculated to confirm minima and transition states, with local minima showing all real frequencies and transition states having one imaginary frequency. IRC calculations ensured correct connectivity between reactants and products.[39] The influence of solvents (water and pentyl ethanoate) was computed with Truhlar's Solvation Model Density (SMD)[40] using the Self-consistent reaction field (SCRF) method. Water (ε = 78.33)

and pentyl ethanoate ($\varepsilon = 4.73$) were chosen as they are highly recommended standard solvents in the literature to mimic the polar and lipid environments in the human body.[41–43]

Three potential mechanisms, namely, HAT, SETPT, and SPLET (as discussed below) have been considered here to explain the antioxidant activity of the hydrazone derivatives.[42,44]

(i) Hydrogen atom transfer (HAT)

$$A - H + R^{\bullet} \rightarrow A^{\bullet} + RH \quad (1)$$

(ii) Single electron transfer followed by proton transfer (SETPT)

$$A - H + R^{\bullet} \rightarrow AH^{\bullet+} + R^{-} \rightarrow A^{\bullet} + RH \quad (2)$$

(iii) Sequential proton loss electron transfer (SPLET)

$$A - H + R^{\bullet} \rightarrow A^{-} + H^{+}; A^{-} + R^{\bullet} \rightarrow A^{\bullet} + RH \quad (3)$$

These mechanisms were defined by intrinsic thermodynamic descriptors, including bond dissociation enthalpy (BDE), ionization energy (IE), proton dissociation enthalpy (PDE), proton affinity (PA), and electron transfer enthalpy (ETE). These values were computed in the gas phase, water, and pentyl ethanoate at 298.15 K and 1 atm using the following expressions:[45]

$$BDE = H(A^{\bullet}) + H(H^{\bullet}) - H(A\text{–}H) \quad (4)$$

$$IE = H(AH^{\bullet+}) + H(e^{-}) - H(A\text{–}H) \quad (5)$$

$$PDE = H(A^{\bullet}) + H(H^{+}) - H(AH^{\bullet+}) \quad (6)$$

$$PA = H(A^{-}) + H(H^{+}) - H(A\text{–}H) \quad (7)$$

$$ETE = H(A^{\bullet}) + H(e^{-}) - H(A^{-}) \quad (8)$$

where H(A–H), $H(A^{\bullet})$, $H(A^{-})$, and $H(AH^{\bullet+})$ are the enthalpies of the parent compound, radical, anion, and cationic radical of the parent compound, respectively. $H(H^{\bullet})$, $H(e^{-})$, and $H(H^{+})$ represent the enthalpies of a hydrogen atom, electron, and proton, respectively. The enthalpies of the proton and electron have been collected from the literature,[46–48] and are reported in Table S1.† The enthalpy of the H$^{\bullet}$ atom was calculated in the gas phase and solvents at the M06-2X/6-311+G(d,p) level of theory.

In this work, the kinetics calculations for the hydroperoxyl and methylperoxyl radical scavenging of hydrazones in the gas phase and water solvent were carried out using the quantum-mechanics-based test for overall free radical scavenging activity (QM-ORSA) protocol. In brief, this methodology separately quantifies the scavenging mechanisms and antioxidant efficiency in both polar (aqueous) and nonpolar (lipid) media, using overall rate coefficients.[41,42] The rate constant (k) for the hydrogen atom transfer reactions was computed in the gas phase using conventional transition state theory (eqn (1))[49,50] (at 298.15 K, 1 M standard state) according to eqn (9) using the Eyringpy program.[51,52]

$$k = \sigma\kappa \frac{k_B T}{h} e^{-(\Delta G^{\ddagger})/RT} \quad (9)$$

where $\Delta G^{\ddagger}$ refers to the Gibbs free energy of activation, k_B and h are the Boltzmann and Planck constants, respectively, σ is the reaction symmetry number, and κ is the tunneling correction, which was calculated using the Eckart asymmetric tunneling method.[53,54]

The Marcus theory was used to estimate the energy barriers of single electron transfer (SET) reactions.[55,56] Eqn (10) and (11) were employed to compute the activation barrier ($\Delta G^{\ddagger}_{SET}$) of SET, which comprises the nuclear reorganization energy (λ) and Gibbs energy of reaction (ΔG°_{SET}) parameter.

$$\Delta G^{\ddagger}_{SET} = \frac{\lambda}{4}\left(1 + \frac{\Delta G^{\circ}_{SET}}{\lambda}\right) \quad (10)$$

$$\lambda = \Delta E_{SET} - \Delta G^{\circ}_{SET} \quad (11)$$

where ΔE_{SET} is the nonadiabatic energy difference between reactants and vertical products.[57]

A correction was applied to rate constants that were close to the diffusion limit in order to obtain realistic results. The apparent rate constants (k_{app}) were determined using the Collins–Kimball theory[58] in solvents at 298.15 K; the steady-state Smoluchowski rate constant (k_D) for an irreversible biomolecular diffusion-controlled reaction was estimated using the literature corresponding to eqn (12) and (13).[59]

$$k_{app} = \frac{k_{TST} k_D}{k_{TST} + k_D} \quad (12)$$

$$k_D = 4\pi R_{AB} D_{AB} N_A \quad (13)$$

where R_{AB} denotes the reaction distance, N_A is the Avogadro number, and D_{AB} is the mutual diffusion coefficient of reactants A and B ($D_{AB} = D_A + D_B$),[58,60] where D_A or D_B is determined using the Stokes–Einstein formulation.[61,62]

$$D_{A\text{ or }B} = \frac{k_B T}{6\pi\eta a_{A\text{ or }B}} \quad (14)$$

η is viscosity of the solvents (*i.e.*, η (water) $= 8.91 \times 10^{-4}$ Pa s), η (pentyl ethanoate) $= 8.62 \times 10^{-4}$ Pa s and $a_{A\text{ or }B}$ is the radius of the corresponding solute A or B.[44]

The solvent cage effects were incorporated according to the correction proposed by Okuno,[63] taking into account the free volume theory following the Benson correction, which was also applied to reduce over-penalizing entropy losses in solution.[41,64,65]

Molecular descriptors such as electronegativity (χ), hardness (η), softness (S), and the electrophilicity index (ω) were calculated using eqn (15)–(18).[66–69]

$$\text{Electronegativity } (\chi) = -\mu \approx (IP + EA)/2 \quad (15)$$

$$\text{Hardness } (\eta) \approx (IP - EA)/2 \quad (16)$$

$$\text{Softness } (S) \approx 1/2\eta \quad (17)$$

$$\text{Electrophilicity index } (\omega) = \mu^2/2\eta \quad (18)$$

The molar fractions of neutral and ionic species for all compounds was obtained by adapting the simple Henderson–Hasselbalch equation into eqn (19) and (20) outlined below.[70]

$$M_f(\text{neutral}) = \frac{[H^+]}{[H^+] + 10^{-pK_a}} \quad (19)$$

$$M_f(\text{anionic}) = \frac{10^{-pK_a}}{[H^+] + 10^{-pK_a}} \quad (20)$$

The pK_a value was calculated using eqn (21)–(23) with an H_2O value is 55.49.[71] The values of ΔG_g, $\Delta G_{solv}(A^-)$, and $\Delta G_{solv}(HA)$ were obtained by SMD M06-2X/6-311+G(d,p) calculations in water, and the solvation free energy of water ($\Delta G_{solv}(H_2O) = -6.32$ kcal mol^{-1}) and hydronium ($\Delta G_{solv}(H_3O^+) = -110.3$ kcal mol^{-1}) have been taken from experimental values.[72]

$$HA + H_2O \rightarrow A^- + H_3O^+ \quad (21)$$

$$\Delta G_{sol} = \Delta G_g + \Delta G_{solv}(A^-) + \Delta G_{solv}(H_3O^+) - \Delta G_{solv}(HA) - \Delta G_{solv}(H_2O) \quad (22)$$

where ΔG_g indicates the Gibbs free energy change associated with the gas phase reaction and computed using the thermodynamic cycle described in the literature.[73] ΔG_{sol} is expressed in units of kcal mol^{-1}.

$$pK_a = \frac{\Delta G_{sol}}{1.364} - \log[H_2O] \quad (23)$$

was corrected in accordance with Pliego using eqn (24).[73]

$$pK_a \text{ (corrected)} = pK_a \text{ (calculated)} - 4.54 \quad (24)$$

Results and discussion

Physicochemical descriptors analysis

Molecular descriptors such as electronegativity (χ), hardness (η), softness (S), and the electrophilicity index (ω) can be employed to examine the electron-donating abilities of hydrazone compounds.[66,74] The computed molecular descriptors have been presented in Table 1.

As can be seen in Table 1, all the investigated hydrazones have relatively comparable values of χ, η, S, and ω in the range of 4.15–5.20, 1.10–3.61, 0.14–0.45, and 3.20–8.37, respectively. These results clearly indicate that in all the studied mediums, hydrazone compounds (**1–6**) prefer to act as electron donors rather than electron acceptors, which is an indication of their radical scavenging activity.[74]

Frontiers molecular orbital (FMO) analysis

The HOMO energy reflects a molecule's electron-donating ability; while its distribution indicates potential sites for free radical attack.[38] The HOMO–LUMO energy gaps for compounds **2**, **4**, and **6** are presented in Fig. 2, while other compounds with high energy gaps are shown in Fig. S2 in the ESI.†

As shown in Fig. 2, all the FMOs show the typical π-type molecular orbital characteristics. The HOMO of all the hydrazone compounds is distributed mainly on the hydrazone moiety and substituted benzene ring, and LUMO orbitals are primarily distributed over the 3,5-dinitrobenzohydrazide ring. The calculated HOMO–LUMO energy gaps follow the order of **6** (4.36 eV) < **2** (4.42 eV) < **4** (4.72 eV) < **1** (5.12 eV) < **5** (5.15 eV) < **3** (5.54 eV). Compounds **6** and **2** exhibit the lowest energy gaps among the compounds, and their values are nearly identical. Therefore, we can conclude that they have comparable reactivity.

Mechanistic study

HAT mechanism. HAT is described by the BDE, which indicates the tendency of H atoms to transfer from antioxidant molecules to free radicals *via* homolytic bond cleavage. Initially, BDE values were computed for all possible X–H (X = O, N, C) bonds in the gas phase (see Table S2, ESI†). Subsequently, the

Table 1 Molecular descriptors (in eV) of the studied compounds **1–6** in the gas phase, water, and pentyl ethanoate computed at M06-2X/6-311+G(d,p) level of theory

Medium	Comp.	Electronegativity (χ)	Hardness (η)	Softness (S)	Electrophilicity index (ω)
Gas phase	**1**	4.94	3.40	0.15	3.59
	2	4.37	2.99	0.17	3.20
	3	5.20	3.61	0.14	3.73
	4	4.98	3.07	0.16	4.04
	5	4.97	3.43	0.15	3.60
	6	4.43	2.99	0.17	3.28
Water	**1**	4.74	1.54	0.32	7.31
	2	4.30	1.10	0.45	8.37
	3	4.93	1.73	0.29	7.04
	4	4.64	1.43	0.35	7.54
	5	4.73	1.53	0.33	7.32
	6	4.34	1.14	0.44	8.25
Pentyl ethanoate	**1**	4.65	2.02	0.25	5.35
	2	4.16	1.58	0.32	5.46
	3	4.84	2.20	0.23	5.33
	4	4.67	1.74	0.29	6.26
	5	4.65	2.02	0.25	5.34
	6	4.15	1.55	0.32	5.53

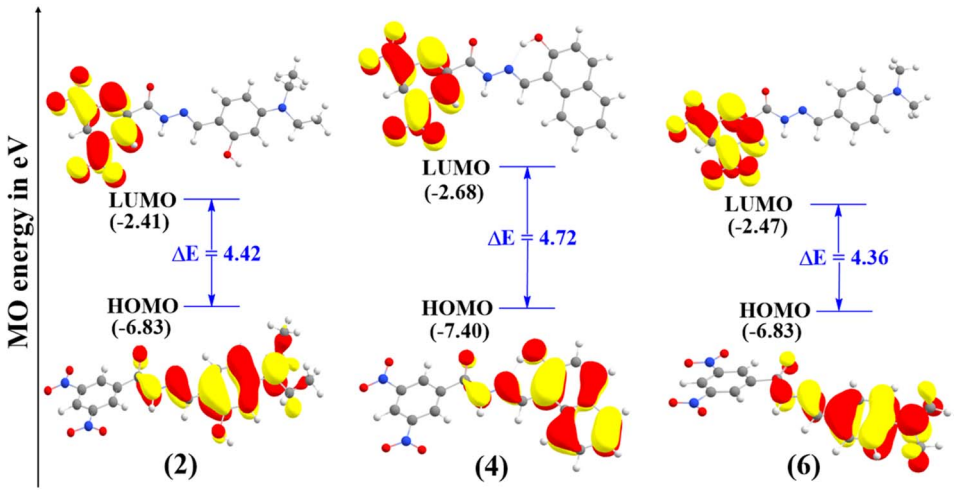

Fig. 2 Frontier molecular orbital (FMO) plots of compound **2**, **4**, and **6** calculated in the gas phase.

lower BDEs of these bonds were calculated in water and pentyl ethanoate solvents to account for solvent effects and presented in Table 2.

Table 2 shows the BDEs of the molecules (**1–6**) in the range of 81.2–96.6 kcal mol^{-1} in the gas phase and solvents. The lowest BDE values were obtained at the O4′–H (Comp. **1**), N8–H (Comp. **4**, **2** and **6**), and O2′–H (Comp. **2**) positions with values ranging from 81.2 to 91.9 kcal mol^{-1} in all phases. The O2′–H BDE of compound **4** is significantly higher (96.6 kcal mol^{-1}) compared to those of other O–H groups (Table S2†), reducing its reactivity. This result can be attributed to an intra-molecular hydrogen bond with the imine nitrogen atom, which elevates the BDE value and is consistent with previous studies.[16] The C–H BDEs are high, ranging from 90.0 to 134.8 kcal mol^{-1}, except for that of the C7′–H bond of compound **2** (88.5 kcal mol^{-1}). This suggests they have a minimal impact on free radical scavenging activity, so all except the C7′–H bond of compound **2** were excluded from further calculations.

Compounds **1** and **2** possess electron-donating –OCH_3 and N–$(CH_2CH_3)_2$ groups on the aromatic ring, which stabilizes the phenoxide radical.[17] Compound **4** has only a hydroxyl group on the naphthalene ring, which may result in hydrogen bonding with the hydrazone moiety. The lowest BDE values of O4′–H (81.2 kcal mol^{-1}), O2′–H (84.8 kcal mol^{-1}), and N8–H (83.3, 84.7 and 84.8 kcal mol^{-1}) in the gas phase of compounds **1**, **2**, **4** and **6** were comparable with the BDE values of other well-known antioxidants such as resveratrol (83.9 kcal mol^{-1}),[75] vanillic acid (85.2 kcal mol^{-1}),[76] puerarin (87.3 kcal mol^{-1}),[77] magnolol (83.1 kcal mol^{-1}),[78] BHA (81.2 kcal mol^{-1}) and other antioxidant polyphenols.[74]

Table 2 Lowest BDE values (in kcal mol^{-1}) of compounds (**1–6**) calculated in the studied environments

		BDE		
Comp.	Site	Gas phase	Water	Pentyl ethanoate
1	N8–H	87.9	94.8	91.4
	O4′–H	81.2	86.5	82.0
2	N8–H	84.7	85.0	83.9
	O2′–H	84.8	86.0	84.6
	C7′–H	88.5	90.4	88.9
3	N8–H	89.4	96.6	93.1
4	N8–H	83.3	91.9	87.4
5	N8–H	87.9	94.2	91.0
	O4′–H	87.1	88.4	86.3
6	N8–H	84.8	87.8	86.1

The spin density distributions of the radical forms (Fig. 3) were calculated in the gas phase to explain the BDE differences. Greater spin delocalization corresponds to easier antioxidant radical formation and lower BDEs. As shown in Fig. 3, the spin density after H-abstraction from O–H bonds is lower than that for N–H bonds, consistent with the BDE values. The most localized radicals were formed after H-abstraction from the C7′–H (Comp. **2**) and N8–H (Comp. 3) bonds, aligning with the BDE results.

SETPT mechanism. As presented in eqn (2), the SETPT mechanism is governed by the ionization potential (IP) of the antioxidant (AH) and the proton dissociation enthalpy (PDE) of the radical cation ($AH^{\bullet+}$). Lower IP and PDE values correspond to higher antioxidant activity through this pathway. The calculated IP and PDE values for compounds **1–6** in the gas phase, water, and pentyl ethanoate are presented in Table 3.

Compounds **2** and **6** exhibit better electron-donor abilities than the others, as predicted by the FMO calculations. Table 3 shows that the IP values in solution are lower than those in the gas phase, following the trend gas phase > pentyl ethanoate > water, likely due to higher electron solvation enthalpies.[74] This suggests that a polar medium enhances electron transfer, promoting free radical scavenging, which is consistent with previous studies.[38]

The lowest PDE values were observed for O4′–H of compound **1** (2.4–211.0 kcal mol^{-1}) and N8–H of compound **3** (5.0–207.8 kcal mol^{-1}) across all media. Compared to those in the gas phase, the PDE values in pentyl ethanoate and water dropped significantly by an average of 207.8 and

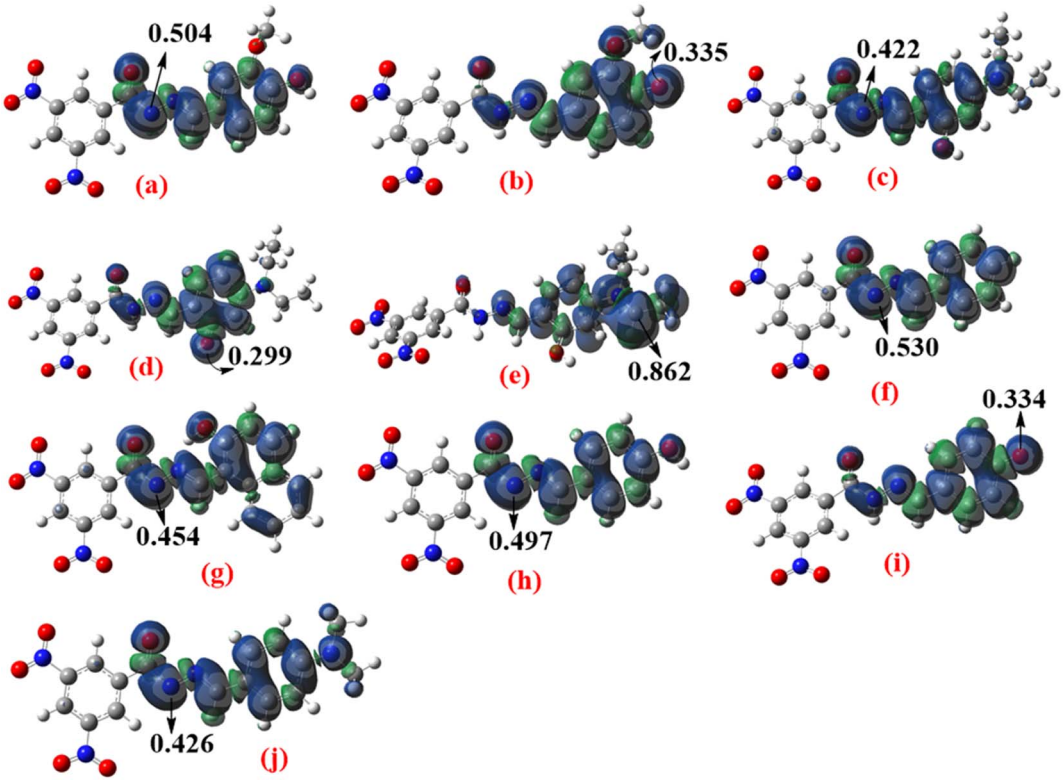

Fig. 3 Spin density distributions of radical forms of the hydrazone compounds obtained after H-abstraction from the following compounds: (a) N8–H and (b) O4′–H of compound **1**; (c) N8–H, (d) O4′–H, and (e) C7′–H of compound **2**; (f) N8–H of compound **3**; (g) N8–H of compound **4**; (h) N8–H and (i) O4′–H of compound **5**; (j) N8–H of compound **6** (arrows and numerical values indicate spin density at specific molecular sites). Calculated at the M062X/6-311+G(d,p) level of theory in the gas phase.

Table 3 Ionization potential (IP) and proton dissociation enthalpy (PDE) values (kcal mol^{-1}) of compounds **1–6** calculated in the studied environments

	IP			PDE			
Compound	Gas phase	Water	Pentyl ethanoate	Site	Gas phase	Water	Pentyl ethanoate
1	183.5	113.2	131.6	N8–H	217.7	13.9	11.8
				O4′–H	211.0	5.6	2.4
2	161.9	94.0	111.7	N8–H	236.1	23.3	24.2
				O2′–H	236.2	24.3	24.9
3	195.0	121.6	140.1	N8–H	207.8	7.3	5.0
4	180.2	111.0	128.6	N8–H	216.5	13.1	10.7
				O2′–H	229.7	13.0	17.3
5	186.0	113.4	132.3	N8–H	215.2	13.1	10.7
				O4′–H	214.4	7.3	6.0
6	166.9	96.1	113.6	N8–H	231.3	24.1	24.5

207.1 kcal mol^{-1}, respectively, due to the high solvation enthalpy of protons in solution, which is consistent with previous studies.[79]

The performance of different mechanisms is generally governed by the enthalpy of the first step. Since the BDE is lower than the IP values, this suggests that the HAT mechanism is thermodynamically more favourable than the SETPT mechanism.

SPLET mechanism. This mechanism is characterized by the values of proton affinity (PA) and electron transfer enthalpy (ETE). In this mechanism, the lower the PA and ETE values, the higher the antioxidant activity. Here, we have calculated the PAs and ETEs for X–H (X = N, O) bonds, and the results are shown in Table 4.

Table 4 demonstrates that compound **4** has the lowest PA value at the N8–H position, with PAs of 309.7 (gas phase), 29.1 (water), and 45.3 (pentyl ethanoate), showing that the proton at this position may be readily deprotonated. In the solution phase, all PA values are significantly lower than in the gas phase, likely due to the large solvation enthalpy of protons. The

Table 4 Proton affinity (PA) and electron transfer enthalpy (ETE) values (kcal mol^{-1}) for all the compounds

		PA			ETE		
Comp.	Site	Gas phase	Water	Pentyl ethanoate	Gas phase	Water	Pentyl ethanoate
1	N8–H	318.4	32.8	51.8	82.9	94.3	91.5
	O4′–H	323.0	30.4	53.6	71.5	88.3	80.4
2	N8–H	323.8	32.8	54.5	74.3	83.7	81.4
	O2′–H	326.5	30.4	56.1	71.6	85.5	80.5
3	N8–H	317.4	32.2	50.8	85.4	96.7	94.4
4	N8–H	309.7	29.1	45.3	87.0	95.1	94.1
	O2′–H	335.4	36.0	63.1	74.5	88.0	82.8
5	N8–H	318.6	32.7	51.6	82.6	93.8	91.4
	O4′–H	325.9	32.2	55.0	74.5	88.5	83.2
6	N8–H	321.7	33.2	52.7	76.5	86.9	85.4

ETE values of the O4′–H (**1**) and O2′–H (**2**) bonds are smaller than those of other bonds in the gas phase and lipid media. In polar solvent, the N8–H and O2′–H bonds of compound **2** have the smallest ETE values. This may be due to the easy movement of electrons from the unstable ions resulting from these bonds. It is also important to note that all of the ETE values are much lower than the corresponding IP values in the examined medium, implying that the anionic forms of hydrazone compounds (**1–6**) have better electron-donating capacity than the neutral forms. These findings are consistent with previous studies.[44,75]

Upon comparing the values of PA, IP, and BDE in Tables 2–4, it is evident that the PA values are lower in water solvent. Hence, it can be concluded that the SPLET mechanism is the thermodynamically dominant mechanism in water.

Reactions of compounds 1–6 with the radical HOO˙. The Gibbs free energies ($\Delta G°$) of the reactions of HOO˙ with all compounds were computed for the first step of each mechanism in the gas phase, and the results are collected in Tables S2 and S3† in the ESI.† The data suggest that H-abstraction is favourable, particularly at the N8–H bonds of all compounds, the C7′–H and O2′–H bond of **2**, the O4′–H bond of **1**, and the O4′–H bond of **5**, as the computed $\Delta G°$ values are negative ($\Delta G° < 0$) or minimal ($\Delta G° < 5$ kcal mol^{-1}).[80] However, the reactions following the single electron transfer (SET) and proton loss (PL) mechanisms are not spontaneous ($\Delta G^{\circ}_{SET} = 139.1 - 172.2$ kcal mol^{-1}, $\Delta G^{\circ}_{PL} = 158.2 - 182.9$ kcal mol^{-1}). Therefore, the HAT mechanism is anticipated to be the primary radical trapping pathway of hydrazone compounds in the gas phase, and thus, this mechanism should be modeled for the kinetic study.

PES of the HAT mechanism for reactions with the radical HOO˙. The PES study focusing on the HAT mechanism is shown in Fig. 4, and the corresponding optimized transition state structures are shown in Fig. 5, S3 and S4 in the ESI.†

The computed energy barriers of all the reactions were in the range of 4.3 to 10.4 kcal mol^{-1}. The lowest energy barriers were observed at TS-2-O2′ and TS-4-N8 at 4.3 and 4.9 kcal mol^{-1}, respectively. This observation aligns with the lowest computed

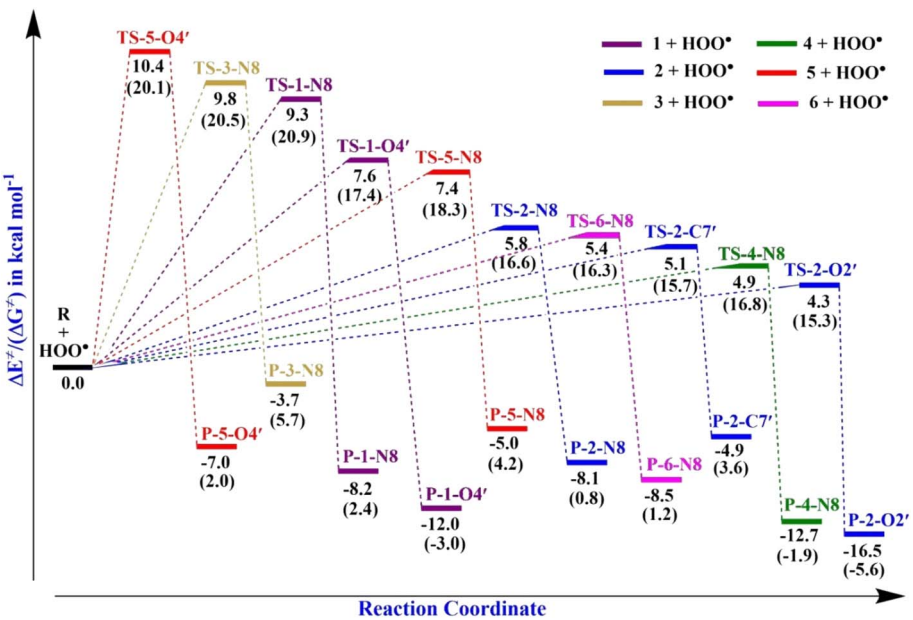

Fig. 4 PES for the reactions of the hydrazone compounds with HOO˙ in the gas phase.

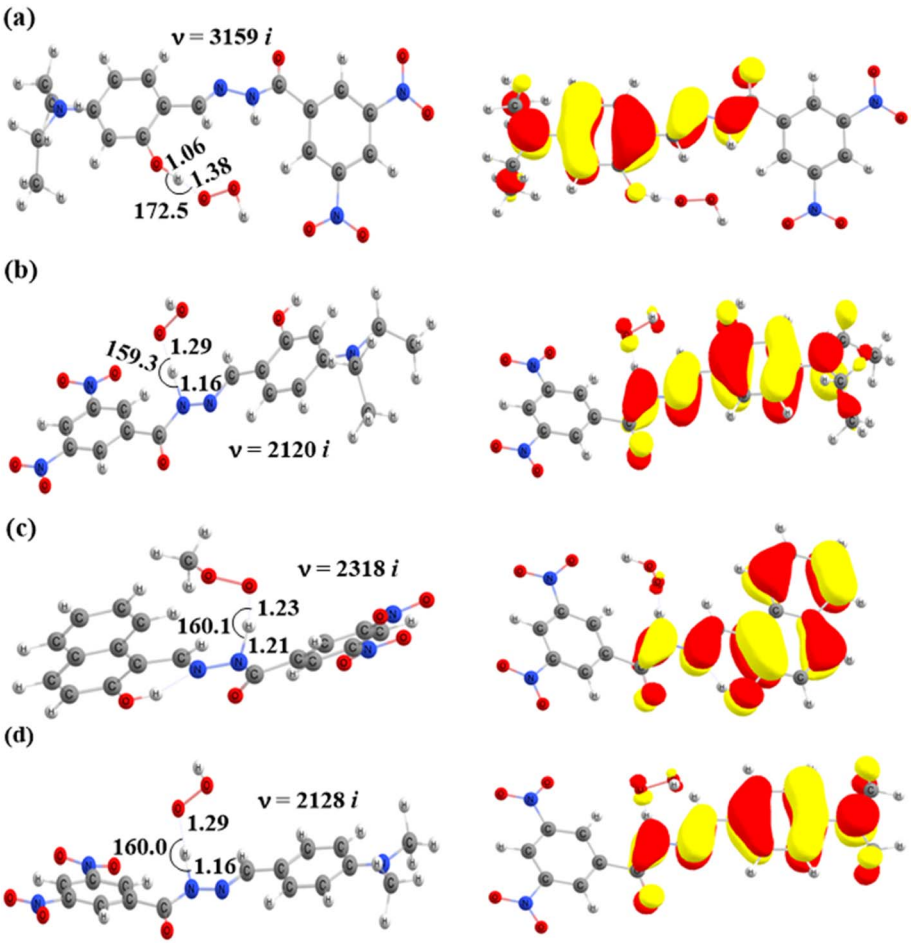

Fig. 5 Optimized geometries of transition states of the HAT reactions between HOO˙ and (a) TS-2-O2′, (b) TS-2-N8, (c) TS-4-N8, and (d) TS-6-N8 and their corresponding SOMO distributions (bond angles in degrees, bond distances in Å).

BDE values at 2-O2′–H (84.8 kcal mol^{-1}) and 4-N8–H (83.3 kcal mol^{-1}). This suggests that the H-abstractions of the HOO˙ radical at O2′ of compound **2** and N8 of compound **4** play a fundamental role in the hydroperoxyl radical scavenging activity.

In addition, the SOMOs of the TSs were examined (Fig. 5 and S3†), in which the atomic orbital aligns with the direction of H-atom transfer, and the electron density appears localized on the donor and acceptor sites.

Reactions of compounds 1–6 with the radical CH_3OO˙. To identify thermodynamically spontaneous pathways, the $\Delta G°$ values for the reaction of the hydrazone derivatives with a CH_3OO˙ radical were calculated for the first step of three typical mechanisms (HAT, SET-PT, and SPLET). The data showed that only the HAT mechanism was spontaneous (Table S2†), specifically at the N8–H bonds of all compounds, the C7′–H bond of **2**, and various O–H bonds in compounds **1**, **2**, and **5** ($\Delta G° = -3.2$ to 4.3 kcal mol^{-1}). In contrast, the SET and SPLET mechanisms were not spontaneous due to high $\Delta G°$ values (Table S3†). Therefore, the HAT pathway is suggested to be the primary mechanism for scavenging CH_3OO˙ in the gas phase, warranting further kinetic study.

PES *via* HAT mechanism for reactions with the radical CH_3OO˙. The thermodynamic analysis revealed that the HAT is the predominant pathway for the reactions of hydrazone compounds (**1–6**) with CH_3OO˙ in the gas phase. Fig. 6 displays the corresponding PES, while the optimized TS structures are shown in Fig. 7, S5 and S6 in the ESI.† As seen in the PES, the energy barriers of the TSs vary from 3.2 to 22.3 kcal mol^{-1}.

TS-2-N8 (3.2 kcal mol^{-1}), TS-2-O2′, (3.6 kcal mol^{-1}) and TS-4-N84.2 (4.2 kcal mol^{-1}) possess very low barriers, as expected based on the BDE results, which indicates that the compounds **2** and **4** have high CH_3OO˙ scavenging activity compared to the others. The breaking bond distances at the TSs are around 1.16–1.41 Å, and the distances for forming bonds (H···OOH) are around 1.03–1.33 Å. The C/N/O···H···O bond angles vary in the range of 154.5 to 170.4°, which indicates the linear arrangements of the atoms around the transferred hydrogen atom. The relative energies of the products were more negative than those of the reactants by about −1.8 to −9.8 kcal mol^{-1}.

Finally, the SOMO density (presented in Fig. 7 and S4†) distributed along the donor–H–acceptor transition vectors confirm the occurrence of the HAT mechanism.

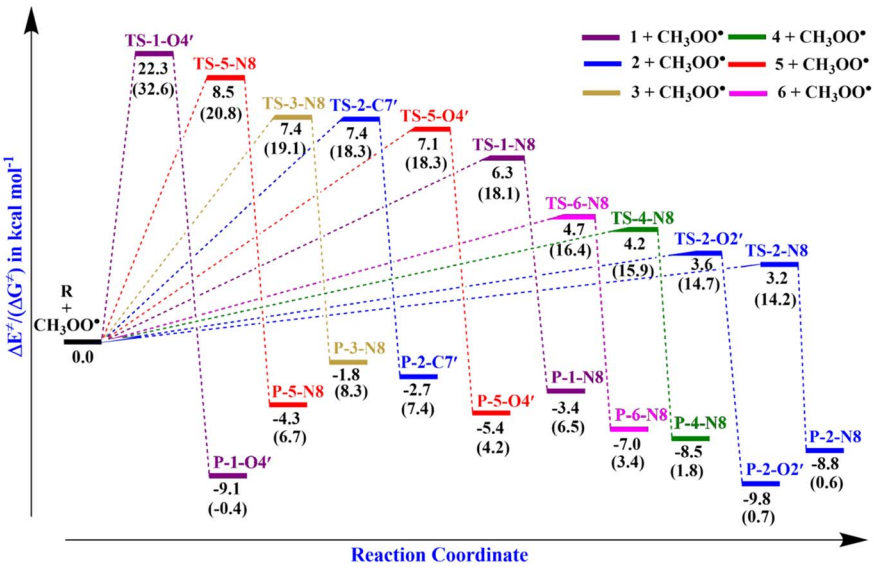

Fig. 6 PES for the hydrazone compounds with $CH_3OO^{\bullet}$ reactions in the gas phase.

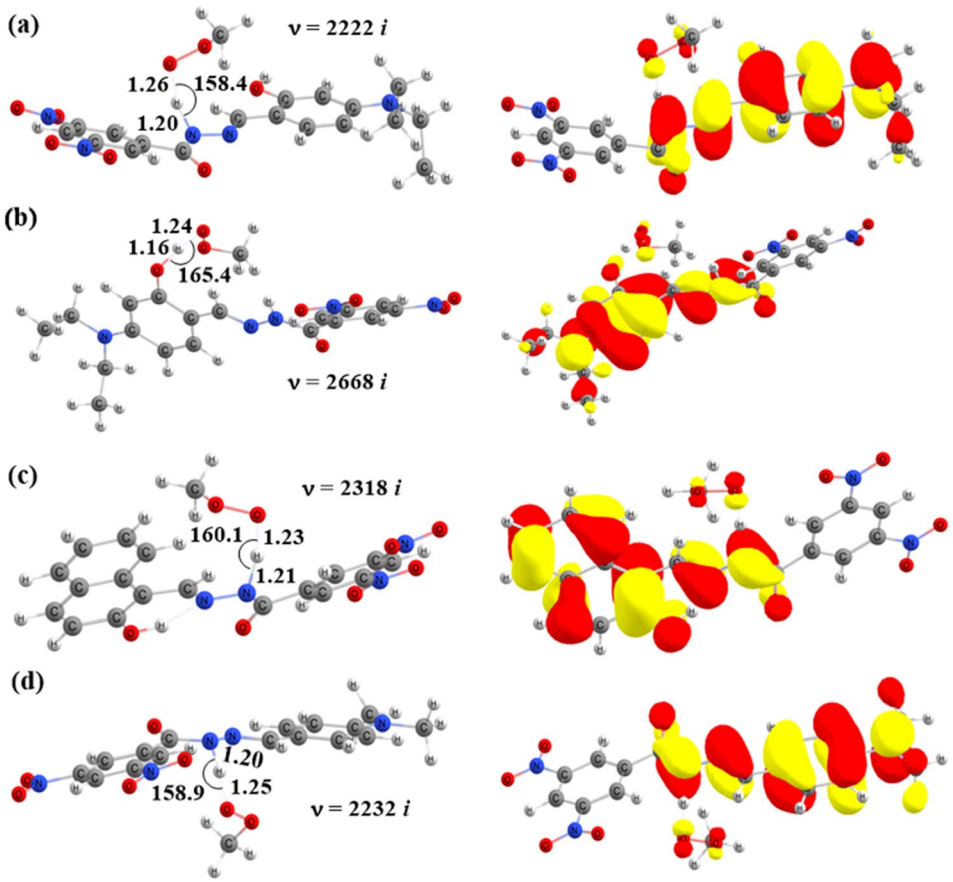

Fig. 7 Optimized geometries of the transition states of HAT reactions between $CH_3OO^{\bullet}$ and (a) TS-2-N8, (b) TS-2-O2′, (c) TS-4-N8, and (d) TS-6-N8 and their corresponding SOMO distributions (bond angles in degrees, bond distances in Å).

Kinetic study

This section employed the QM-ORSA protocol[41,42] to analyse the kinetics of hydroperoxyl and methylperoxyl radical scavenging of the studied compounds in the gas phase following the HAT mechanism. The data presented in Table 5 indicate that the rate constant values for reactions involving the HOO• radical fall

Table 5 Gibbs free energy of activation ($\Delta G^{\ddagger}$ in kcal mol^{-1}), tunnelling corrections (κ), and rate constant (k_{Eck}, M^{-1} s^{-1}) for the HOO$^{\bullet}$ and $CH_3OO^{\bullet}$ scavenging of hydrazone compounds **1–6** computed in the gas phase

		HOO$^{\bullet}$				$CH_3OO^{\bullet}$			
Comp.	Position	$\Delta G^{\ddagger}$	κ	k_{Eck}	$k_{overall}$	$\Delta G^{\ddagger}$	κ	k_{Eck}	$k_{overall}$
1	N8–H	20.9	1974.3	1.51×10^{2}	4.85×10^{3}	18.1	63.6	5.24×10^{2}	5.24×10^{2}
	O4′–H	17.4	178.8	4.70×10^{3}		32.6	4.4	8.43×10^{-10}	
2	N8–H	16.6	43.3	4.70×10^{3}	6.86×10^{4}	14.2	14.5	9.03×10^{4}	1.63×10^{5}
	O2′–H	15.3	69.5	6.02×10^{4}		14.7	29.3	7.22×10^{4}	
	C7′–H	15.7	3.9	3.67×10^{3}		18.3	10.7	1.20×10^{2}	
3	N8–H	20.5	417.5	6.02×10^{1}	6.02×10^{1}	19.1	83.6	1.26×10^{2}	1.26×10^{2}
4	N8–H	16.8	101.8	7.83×10^{3}	7.83×10^{3}	15.9	29.0	1.08×10^{4}	1.08×10^{4}
5	N8–H	18.3	90.1	5.24×10^{2}	1.49×10^{3}	20.8	596.1	5.54×10^{1}	1.02×10^{3}
	O4′–H	20.1	3334.5	9.63×10^{2}		18.3	158.9	9.63×10^{2}	
6	N8–H	16.3	38.0	6.02×10^{3}	6.02×10^{3}	16.4	34.7	5.24×10^{3}	5.24×10^{3}
BHA	O–H	12.9	4.7	2.41×10^{5}	2.41×10^{5}	15.7	146.1	6.62×10^{4}	6.62×10^{4}

between 6.02×10^{1} to 6.02×10^{4} M^{-1} s^{-1}, whereas the $\Delta G^{\ddagger}$ values range from 15.3 to 20.9 kcal mol^{-1}. The tunnelling corrections (κ) vary from 3.9 to 3334.5, significantly impacting the rate constant. The highest rate constant was observed for the H-abstraction at O2′–H (**2**) with a k_{Eck} value of 6.02×10^{4} M^{-1} s^{-1} ($\Delta G^{\ddagger} = 15.3$ kcal mol^{-1}). Nevertheless, the values for compounds **6** and **2** were 6.02×10^{3} M^{-1} s^{-1} (N8–H, $\Delta G^{\ddagger} = 16.3$ kcal mol^{-1} **6**), 4.70×10^{3} M^{-1} s^{-1} (N8–H, $\Delta G^{\ddagger} = 16.2$ kcal mol^{-1} **2**), and 3.67×10^{3} M^{-1} s^{-1} (C7′–H, $\Delta G^{\ddagger} = 15.7$ kcal mol^{-1} **2**), which are lower than those for compound **4** ($k_{Eck} = 7.83 \times 10^{3}$ M^{-1} s^{-1}), even though the reaction barrier for the 4-N8–H + HOO$^{\bullet}$ reaction ($\Delta G^{\ddagger} = 16.8$ kcal mol^{-1}) is higher than that of these reactions. This apparent disparity can be elucidated by the tunneling correction for the H-abstraction at the N8–H (**4**) bond ($\kappa = 101.8$) in comparison to those for the N8–H (**6**) ($\kappa = 38.0$), N8–H (**2**) ($\kappa = 43.3$), and C7′–H (**2**) bonds ($\kappa = 3.9$).

Conversely, the H-abstractions involving the $CH_3OO^{\bullet}$ radical exhibited the highest rate constants on the N8–H (**2**, **4**) and O2′–H (**2**) bonds with k_{Eck} values of 9.03×10^{4} M^{-1} s^{-1} ($\Delta G^{\ddagger} = 14.2$ kcal mol^{-1}, **2**), 1.08×10^{4} M^{-1} s^{-1} ($\Delta G^{\ddagger} = 15.9$ kcal mol^{-1}, **2**) and 7.22×10^{4} M^{-1} s^{-1} ($\Delta G^{\ddagger} = 14.7$ kcal mol^{-1}, **4**), respectively. The overall rate constants for the reactions of compounds **2** and **4** with $CH_3OO^{\bullet}$ are often higher than those with the HOO$^{\bullet}$ radical. This is owing to a smaller reaction energy barrier for reactions *via* the $CH_3OO^{\bullet}$ radical than *via* HOO$^{\bullet}$. Based on the computed data, compounds **2** and **4** have faster HOO$^{\bullet}$ and $CH_3OO^{\bullet}$ radical scavenging activity in the gas phase than typical antioxidants like umbelliferone (4.57×10^{1} M^{-1} s^{-1}),[81] artepillin C (3.49×10^{2} M^{-1} s^{-1}),[82] 3-pyrroline-2-ones (5.48×10^{1} M^{-1} s^{-1})[83] and natural depsidones (1.37 M^{-1} s^{-1}).[84]

Furthermore, Başaran *et al.*[28] performed experimental investigations and discovered that compound **2** exhibited better antioxidant activity compared to BHA, followed by that of compound **4**. As per the aforementioned discussion, our results are in excellent agreement with these findings.

Radical scavenging activity of hydrazones in aqueous solutions

Acid–base equilibria. Prior studies have suggested that deprotonation can significantly influence the efficacy of antioxidants in aqueous solutions.[41,51,85] The lowest PA values were identified at the O–H bonds of compounds **1**, **2**, and **5** and the N–H bonds of compounds **3**, **4**, and **6** in aqueous solution; these bonds were subsequently utilized to calculate the pK_a values for the examined compounds. The calculated pK_a values (Table 6) range from 4.66–7.71. At pH = 7.4, the molar fraction values of the neutral form M_f (AH) range from 0.002–0.671, and those of the anionic form M_f (A^-) range from 0.329–0.998.

Table 6 Calculated pK_a values and molar fractions (M_f) of the neutral (AH) and anionic (A^-) species at pH = 7.4 in water solvent

Comp.	Position	pK_a	M_f (AH)	M_f (A^-)
1	O4′–H	5.64	0.017	0.983
2	O2′–H	7.41	0.506	0.494
3	N8–H	6.95	0.262	0.738
4	N8–H	4.66	0.002	0.998
5	O4′–H	6.96	0.266	0.734
6	N8–H	7.71	0.671	0.329

The SET mechanism in its neutral form is non-spontaneous, showing a significantly positive reaction free energy (ΔG°) (Table S4†). For the anionic forms, although ΔG° remains slightly positive rather than negative, this could still contribute to the radical scavenging activity, as suggested by previous reports.[15]

Marcus' theory was used to evaluate the kinetic parameters such as $\Delta G^{\neq}_{SET}$ (activation barrier), λ (nuclear reorganization energy) and rate constants (k_{app}, k_f) of the reaction between anions of the studied compounds with the typical radicals HOO$^{\bullet}$ and $CH_3OO^{\bullet}$ following the SET mechanism. As shown in Table 7, the hydroperoxyl and methoxy peroxyl radical scavenging activity is greatest for the anion of compound **2** with $k_{app} = 1.8 \times 10^{7}$ M^{-1} s^{-1} ($\Delta G^{\neq}_{SET} = 7.6$ kcal mol^{-1}) and $k_{app} = 3.3 \times 10^{6}$ M^{-1} s^{-1} ($\Delta G^{\neq}_{SET} = 8.6$ kcal mol^{-1}), respectively. Compounds **1**, **4**, **5**, and **6** exhibited moderate radical scavenging behaviour following the SET mechanism ($k_{app} = 10^{2}$–10^{6} M^{-1} s^{-1}). Conversely, compound **3** shows very low antioxidant activity ($k_{app} = 10^{1}$ M^{-1} s^{-1}). Based on the calculated data, we can conclude that compound **2** showed better HOO$^{\bullet}$ and $CH_3OO^{\bullet}$ radical scavenging activity compared to some typical antioxidants such as rubiadin [1.50

Table 7 Calculated $\Delta G^{\ddagger}_{SET}$ (kcal mol^{-1}), λ (kcal mol^{-1}), k_{app} (M^{-1} s^{-1}), M_f, and k_f (M^{-1} s^{-1}) values of the studied compounds (**1–6**) with HOO$^{\bullet}$ and $CH_3OO^{\bullet}$ radicals in water solvent

Radical	Comp.	Position	$\Delta G^{\neq}_{SET}$	λ	k_{app}	M_f	k_f
HOO$^{\bullet}$	**1**	O4′–H	8.2	15.2	6.3×10^6	0.983	6.2×10^6
	2	O2′–H	7.6	21.2	1.8×10^7	0.494	8.9×10^6
	3	N8–H	15.1	20.4	5.0×10^1	0.738	3.7×10^1
	4	N8–H	14.3	20.0	2.1×10^2	0.998	2.1×10^2
	5	O4′–H	9.6	20.3	5.7×10^5	0.734	4.2×10^5
	6	N8–H	8.8	21.5	2.3×10^6	0.329	7.6×10^5
$CH_3OO^{\bullet}$	**1**	O4′–H	9.5	14.7	7.2×10^5	0.983	7.1×10^5
	2	O2′–H	8.6	20.7	3.3×10^6	0.494	1.6×10^6
	3	N8–H	16.7	19.9	3.7×10^0	0.738	2.7×10^0
	4	N8–H	15.8	19.5	1.7×10^1	0.998	1.7×10^1
	5	O4′–H	10.8	19.9	7.9×10^4	0.734	5.8×10^4
	6	N8–H	9.9	21.0	3.7×10^5	0.329	1.2×10^5

(HOO$^{\bullet}$), 4.5×10^{-2} M^{-1} s^{-1} ($CH_3OO^{\bullet}$)],[30] natural fraxin [(HOO$^{\bullet}$) 6.7×10^3, 4.2×10^2 M^{-1} s^{-1} ($CH_3OO^{\bullet}$)],[86] and natural anthraquinones [2.10×10^2 M^{-1} s^{-1}($CH_3OO^{\bullet}$)][87] in water at pH = 7.4.

Conclusion

In this work, a systematic DFT investigation of the HOO$^{\bullet}$ and $CH_3OO^{\bullet}$ radical scavenging activity of six hydrazone compounds has been reported. The mechanism has been studied based on a thermodynamic perspective utilizing three distinct pathways: HAT, SETPT, and SPLET, alongside their corresponding molecular descriptors, including BDE, IP, PDE, PA, and ETE. The results show that HAT is most favorable in the gas phase, while SPLET is preferred in a polar medium. The O2′–H and N8–H bonds play a decisive role in the radical scavenging of compound **2**. Among the studied compounds, compound **2** showed the highest rate constants for HOO$^{\bullet}$ scavenging *via* the HAT mechanism in the gas phase at the O2′–H site ($k = 6.02 \times 10^4$ M^{-1} s^{-1}). For $CH_3OO^{\bullet}$ scavenging, it achieved peak rates at the N8–H (9.03×10^4 M^{-1} s^{-1}) and O2′–H (7.22×10^4 M^{-1} s^{-1}) sites. The calculated overall rate constant values for the HOO$^{\bullet}$ and $CH_3OO^{\bullet}$ radical scavenging of compound **2** are 6.86×10^4 M^{-1} s^{-1} and 1.63×10^5 M^{-1} s^{-1}, respectively. These findings, which are consistent with the experimental data, suggest antioxidant activity comparable to that of butylated hydroxyanisole (BHA). In aqueous solution, the anionic form of compound **2** displayed the highest radical scavenging rates among the tested compounds, with k_{app} values of 1.8×10^7 M^{-1} s^{-1} for HOO$^{\bullet}$ and 3.3×10^6 M^{-1} s^{-1} for $CH_3OO^{\bullet}$, outperforming antioxidants like rubiadin and natural anthraquinones. Thus, compound **2** shows promise as an effective antioxidant in aqueous physiological environments.

Data availability

The data supporting this article have been included as part of the ESI.†

Conflicts of interest

There are no conflicts to declare.

References

1 A. M. Pisoschi and A. Pop, *Eur. J. Med. Chem.*, 2015, **97**, 55–74.
2 V. Lobo, A. Patil, A. Phatak and N. Chandra, *Pharmacogn. Rev.*, 2010, **4**, 118–126.
3 L. A. Pham-Huy, H. He and C. Pham-Huy, *Int. J. Biomed. Sci.*, 2008, **4**, 89–96.
4 S. K. Bardaweel, M. Gul, M. Alzweiri, A. Ishaqat, H. A. Alsalamat and R. M. Bashatwah, *Eurasian J. Med.*, 2018, **50**, 193–201.
5 F. Magnani and A. Mattevi, *Curr. Opin. Struct. Biol.*, 2019, **59**, 91–97.
6 M. Hayyan, M. A. Hashim and I. M. Alnashef, *Chem. Rev.*, 2016, **116**, 3029–3085.
7 Q. V. Vo, P. C. Nam, M. V. Bay, N. M. Thong, L. T. Hieu and A. Mechler, *RSC Adv.*, 2019, **9**, 42020–42028.
8 C. Iuga, J. R. Alvarez-Idaboy and N. Russo, *J. Org. Chem.*, 2012, **77**, 3868–3877.
9 H. Jabeen, S. Saleemi, H. Razzaq, A. Yaqub, S. Shakoor and R. Qureshi, *J. Photochem. Photobiol., B*, 2018, **180**, 268–275.
10 I. Gülçin, *J. Med. Food*, 2011, **14**, 975–985.
11 M. V. Bay, N. M. Thong, P. C. Nam, A. Mechler, N. T. Hoa and Q. V. Vo, *Chem. Phys. Lett.*, 2023, **832**, 140867.
12 N. M. Thong, Q. V. Vo, T. L. Huyen, M. V. Bay, D. Tuan and P. C. Nam, *ACS Omega*, 2019, **4**, 14996–15003.
13 T. D. Ngoc, T. N. Le, T. V. A. Nguyen, A. Mechler, N. T. Hoa, N. L. Nam and Q. V. Vo, *J. Phys. Chem. B*, 2022, **126**, 702–707.
14 C. Kaur and D. Mandal, *Comput. Theor. Chem.*, 2023, **1219**, 113973.
15 M. K. Georgieva, N. Anastassova, D. Stefanova and D. Yancheva, *J. Phys. Chem. B*, 2023, **127**, 4364–4373.
16 N. G. Hristova-Avakumova, E. P. Valcheva, N. O. Anastassova, B. I. Nikolova-Mladenova, L. A. Atanasova, S. E. Angelova and D. Y. Yancheva, *J. Mol. Struct.*, 2021, **1245**, 131021.
17 H. S. Kareem, A. Ariffin, N. Nordin, T. Heidelberg, A. Abdul-Aziz, K. W. Kong and W. A. Yehye, *Eur. J. Med. Chem.*, 2015, **103**, 497–505.
18 N. O. Can, D. Osmaniye, S. Levent, B. N. Sağlik, B. Inci, S. Ilgin, Y. Özkay and Z. A. Kaplancikli, *Molecules*, 2017, **22**, 1381–1400.
19 I. F. Nassar, A. F. EI Farargy, F. M. Abdelrazek and Z. Hamza, *Nucleosides, Nucleotides Nucleic Acids*, 2020, **39**, 991–1010.
20 Z. Peng, G. Wang, Q. H. Zeng, Y. Li, Y. Wu, H. Liu, J. J. Wang and Y. Zhao, *Food Chem.*, 2021, **341**, 128265.
21 B. B. Kashid, J. T. Kilbile, K. D. Wani, S. M. Pawar, V. M. Khedkar and A. A. Ghanwat, *Comb. Chem. High Throughput Screen.*, 2020, **25**, 274–283.
22 A. Baier, A. Kokel, W. Horton, E. Gizińska, G. Pandey, R. Szyszka, B. Török and M. Török, *ChemMedChem*, 2021, **16**, 1927–1932.
23 S. A. Aly and S. K. Fathalla, *Arab. J. Chem.*, 2020, **13**, 3735–3750.
24 E. Bozkurt, Y. Sıcak, E. E. Oruç-Emre, A. K. Iyidoğan and M. Öztürk, *Russ. J. Bioorg. Chem.*, 2020, **46**, 702–714.

25 N. Afriana, N. Frimayanti, A. Zamri and J. Jasril, *J. Phys.:Conf. Ser.*, 2020, **1655**, 012036.
26 B. R. Thorat, A. Gurav, B. Dalvi, A. Sawant, V. Lokhande and S. N. Mali, *Curr. Chin. Chem.*, 2020, **1**, 30–46.
27 N. A. Alsaif, M. A. Bhat, M. A. Al-Omar, H. M. Al-Tuwajiri, A. M. Naglah and A. Al-Dhfyan, *J. Chem.*, 2020, **2020**, 4916726.
28 E. Başaran, N. Haşimi, R. Çakmak and E. Çınar, *Russ. J. Bioorg. Chem.*, 2022, **48**, 143–152.
29 I. A. Khodja, C. Bensouici and H. Boulebd, *J. Mol. Struct.*, 2020, **1221**, 128858.
30 L. T. Hieu, N. T. Hoa, A. Mechler and Q. V. Vo, *J. Phys. Chem. B*, 2023, **127**, 11045–11053.
31 L. T. Hieu, M. Van Bay, N. T. Hoa, A. Mechler and Q. V. Vo, *RSC Adv.*, 2022, **12**, 32693–32699.
32 M. J. Frisch, G. W. Trucks, H. B. Schlegel, G. E. Scuseria, M. A. Robb, J. R. Cheeseman, G. Scalmani, V. Barone, B. Mennucci, G. A. Petersson, H. Nakatsuji, M. Caricato, X. Li, H. P. Hratchian, A. F. Izmaylov, G. Z. J. Bloino, J. L. Sonnenberg, M. Hada, M. Ehara, K. Toyota, R. Fukuda, J. Hasegawa, M. Ishida, T. Nakajima, Y. Honda, O. Kitao, H. Nakai, T. Vreven, J. A. Montgomery Jr, J. E. Peralta, F. Ogliaro, M. Bearpark, J. J. Heyd, E. Brothers, K. N. Kudin, V. N. Staroverov, T. Keith, R. Kobayashi, J. Normand, K. Raghavachari, A. Rendell, J. C. Burant, S. S. Iyengar, J. Tomasi, M. Cossi, N. Rega, J. M. Millam, M. Klene, J. E. Knox, J. B. Cross, V. Bakken, C. Adamo, J. Jaramillo, R. Gomperts, R. E. Stratmann, O. Yazyev, A. J. Austin, R. Cammi, C. Pomelli, J. W. Ochterski, R. L. Martin, K. Morokuma, V. G. Zakrzewski, G. A. Voth, P. Salvador, J. J. Dannenberg, S. Dapprich, A. D. Daniels, O. Farkas, J. B. Foresman, J. V. Ortiz, J. Cioslowski and D. J. Fox, *Gaussian 16*, Revision B.01, Gaussian, Inc., Wallingford, CT, 2016.
33 Y. Zhao and D. G. Truhlar, *Theor. Chem. Acc.*, 2008, **120**, 215–241.
34 H. Boulebd, I. A. Khodja, M. V. Bay, N. T. Hoa, A. Mechler and Q. V. Vo, *J. Phys. Chem. B*, 2020, **124**, 4123–4131.
35 H. Boulebd, A. Mechler, N. T. Hoa and Q. V. Vo, *New J. Chem.*, 2020, **44**, 9863.
36 L. T. Hieu, M. V. Bay, N. T. Hoa, A. Mechler and Q. V. Vo, *RSC Adv.*, 2022, **12**, 32693.
37 D. Mandal, C. Sahu, S. Bagchi and A. K. Das, *J. Phys. Chem. A*, 2013, **117**, 3739–3750.
38 C. Kaur and D. Mandal, *Theor. Chem. Acc.*, 2024, **143**, 28.
39 C. Gonzalez and H. B. Schlegel, *J. Chem. Phys.*, 1991, **95**, 5853–5860.
40 A. V. Marenich, C. J. Cramer and D. G. Truhlar, *J. Phys. Chem. B*, 2009, **113**, 6378–6396.
41 A. Galano and J. R. Alvarez-Idaboy, *J. Comput. Chem.*, 2013, **34**, 2430–2445.
42 A. Galano and J. Raúl Alvarez-Idaboy, *Int. J. Quantum Chem.*, 2019, **119**, e25665.
43 D. Q. Dao, T. T. T. Phan, T. L. A. Nguyen, P. T. H. Trinh, T. T. Van Tran, J. S. Lee, H. J. Shin and B.-K. Choi, *J. Chem. Inf. Model.*, 2020, **60**, 1329–1351.
44 C. Kaur and D. Mandal, *Struct. Chem.*, 2024, 1–11.
45 Y. Shang, H. Zhou, X. Li, J. Zhou and K. Chen, *New J. Chem.*, 2019, **43**, 15736–15742.
46 J. J. Fifen, *J. Chem. Theory Comput.*, 2013, **9**, 3165–3169.
47 J. J. Fifen, Z. Dhaouadi and M. Nsangou, *J. Phys. Chem. A*, 2014, **118**, 11090–11097.
48 Z. Marković, J. Tošović, D. Milenković and S. Marković, *Comput. Theor. Chem.*, 2016, **1077**, 11–17.
49 M. G. Evans and M. Polanyi, *Trans. Faraday Soc.*, 1935, **31**, 875–894.
50 H. Eyring, *J. Chem. Phys.*, 1935, **3**, 107–115.
51 E. Dzib, J. L. Cabellos, F. Ortíz-Chi, S. Pan, A. Galano and G. Merino, *Int. J. Quantum Chem.*, 2019, **119**, e25686.
52 E. Dzib, A. Quintal, F. Ortiz-Chi and G. Merino, *Eyringpy 2.0*, Cinvestav, Merida, Yucatan, 2021.
53 C. Eckart, *Phys. Rev.*, 1930, **35**, 1303.
54 R. Jaglan and D. Mandal, *Comput. Theor. Chem.*, 2020, **1187**, 112920.
55 R. A. Marcus, *Annu. Rev. Phys. Chem.*, 1964, **15**, 155–196.
56 R. A. Marcus, *Rev. Mod. Phys.*, 1993, **65**, 599.
57 S. F. Nelsen, S. C. Blackstock and Y. Kim, *J. Am. Chem. Soc.*, 1987, **109**, 677–682.
58 F. C. Collins and G. E. Kimball, *J. Colloid Sci.*, 1949, **4**, 425–437.
59 M. Von Smoluchowski, *Z. Phys. Chem.*, 1917, **92**, 129–168.
60 D. G. Truhlar, *J. Chem. Educ.*, 1985, **62**, 104.
61 G. G. Stokes, *Mathematical and Physical Papers*, University Press, Cambridge, 1905.
62 A. Einstein, *Ann. Phys.*, 1905, **17**, 549–560.
63 Y. Okuno, *Chem.–Eur. J.*, 1997, **3**, 212–218.
64 S. Benson, *The Foundations of Chemical Kinetics*, Malabar, Florida, 1982.
65 J. R. Alvarez-Idaboy, L. Reyes and N. Mora-Diez, *Org. Biomol. Chem.*, 2007, **5**, 3682–3689.
66 R. G. Parr, L. V. Szentpaly and S. Liu, *J. Am. Chem. Soc.*, 1999, **121**, 1922–1924.
67 R. G. Parr and R. G. Pearson, *J. Am. Chem. Soc.*, 1983, **105**, 7512–7516.
68 W. Kohn, A. D. Becke and R. G. Parr, *J. Phys. Chem.*, 1996, **100**, 12974–12980.
69 P. K. Chattaraj, H. Lee and R. G. Parr, *J. Am. Chem. Soc.*, 1991, **113**, 1855–1856.
70 R. A. Rusdipoetra, H. Suwito, N. N. T. Puspaningsih and K. U. Haq, *RSC Adv.*, 2024, **14**, 6310–6323.
71 S. A. McKee and T. V. Pogorelov, *Gaussian 09*, University of Illinois, Urbana-Champaign, 2019.
72 J. R. Pliego Jr and J. M. Riveros, *Phys. Chem. Chem. Phys.*, 2002, **4**, 1622–1627.
73 J. R. Pliego Jr, *Chem. Phys. Lett.*, 2003, **367**, 145–149.
74 Y. Z. Zheng, G. Deng, Q. Liang, D.-F. Chen, R. Guo and R.-C. Lai, *Sci. Rep.*, 2017, **7**, 7543.
75 Y. Shanga, H. Zhoua, X. Li, J. Zhoua and K. Chen, *New J. Chem.*, 2019, **43**, 15736–15742.
76 C.-H. Hsu, Y. M. Hung, K.-A. Chu, C.-F. Chen, C.-H. Yin and C.-C. Lee, *Sci. Rep.*, 2020, **10**, 1–10.
77 H. Zhou, X. Li, Y. Shang and K. Chen, *Antioxidants*, 2019, **8**, 590.

78 J. Sharanya, A. Purushothaman, D. Janardanan and K. Koley, *Comput. Theor. Chem.*, 2024, **1232**, 114460.
79 M. Spiegel, *J. Phys. Chem. B*, 2023, **127**, 8769–8779.
80 L. T. Hieu, M. V. Bay, N. T. Hoa, A. Mechler and Q. V. Vo, *RSC Adv.*, 2022, **22**, 32693–32699.
81 H. Boulebd, *Phytochemistry*, 2021, **184**, 112670.
82 H. Boulebd, A. Mechler, N. T. Hoa, P. C. Nam, D. T. Quang and Q. V. Vo, *New J. Chem.*, 2021, **45**, 7774–7780.
83 N. T. Nguyen, V. V. Dai, A. Mechler, N. T. Hoa and Q. V. Vo, *RSC Adv.*, 2022, **12**, 24579–24588.
84 M. Van Bay, P. C. Nam, D. T. Quang, A. Mechler, N. K. Hien, N. T. Hoa and Q. V. Vo, *ACS Omega*, 2020, **5**, 7895–7902.
85 N. M. Tam, N. M. Thong, T. Le Huyen, L. P. Hoang, A. Mechler and Q. V. Vo, *J. Mol. Graphics Modell.*, 2021, **105**, 107892.
86 P. C. Nam, N. M. Thong, N. T. Hoa, D. T. Quang, L. P. Hoang, A. Mechler and Q. V. Vo, *RSC Adv.*, 2021, **11**, 14269–14275.
87 N. Q. Trung, N. M. Thong, D. H. Cuong, T. D. Manh, L. P. Hoang, N. K. Hien, P. C. Nam, D. T. Quang, A. Mechler and Q. V. Vo, *ACS Omega*, 2021, **6**, 13391–13397.